single electron-hole pairs efficiently (*25*). The vertical coupling efficiency out of the cavity should be also improved by proper modifications of the cavity structure, e.g., the size of the air holes (*26*) and/or the reflectivity of the substrate. Alternatively, the photons localized in the cavity could be funneled horizontally into the neighboring low-loss photonic crystal waveguide (*27*) prepared by the quantum well intermixing (*28*). Together with all the challenging issues, the demonstration of electrically driven single-cell photonic crystal laser is believed to represent a small but meaningful step toward the ultimate photon source.

References and Notes

1. K. J. Vahala, *Nature* **424**, 839 (2003).
2. E. Yablonovitch, *Phys. Rev. Lett.* **58**, 2059 (1987).
3. T. F. Krauss, R. M. De La Rue, *Prog. Quantum Electron.* **23**, 51 (1999).
4. O. Painter *et al.*, *Science* **284**, 1819 (1999).
5. H. G. Park *et al.*, *Appl. Phys. Lett.* **79**, 3032 (2001).
6. H. Y. Ryu *et al.*, *Appl. Phys. Lett.* **80**, 3883 (2002).
7. M. Loncar, T. Yoshie, A. Scherer, P. Gogna, Y. Qiu, *Appl. Phys. Lett.* **81**, 2680 (2002).
8. K. Srinivasan *et al.*, *Appl. Phys. Lett.* **83**, 1915 (2003).
9. W. D. Zhou *et al.*, *IEEE J. Quantum Electron.* **37**, 1153 (2001).
10. D. S. Song, S. H. Kim, H. G. Park, C. K. Kim, Y. H. Lee, *Appl. Phys. Lett.* **80**, 3901 (2002).
11. T. D. Happ *et al.*, *Appl. Phys. Lett.* **82**, 4 (2003).
12. S. Noda, M. Yokoyama, M. Imada, A. Chutinan, M. Mochizuki, *Science* **293**, 1123 (2001).
13. R. Colombelli *et al.*, *Science* **302**, 1374 (2003); published online 30 October 2003; 10.1126/science.1090561.
14. A. F. J. Levi *et al.*, *Electron. Lett.* **28**, 1010 (1992).
15. H. G. Park *et al.*, *IEEE J. Quantum Electron.* **38**, 1353 (2002).
16. H. G. Park *et al.*, *IEEE Photonics Technol. Lett.* **15**, 1327 (2003).
17. Materials and methods are available as supporting material on *Science* Online.
18. The large thermal resistance (346 K mW^{-1}) of the post structure is responsible for this small duty cycle.
19. M. Fujita, R. Ushigome, T. Baba, *IEEE Photonics Technol. Lett.* **13**, 403 (2001).
20. R. E. Slusher *et al.*, *Appl. Phys. Lett.* **63**, 1310 (1993).
21. H. Yokoyama, *Science* **256**, 66 (1992).
22. J. Vuckovic *et al.*, *IEEE J. Quantum Electron.* **35**, 1168 (1999).
23. L. A. Coldren, S. W. Corzine, *Diode Lasers and Photonic Integrated Circuits* (Wiley, New York, 1995).
24. Z. Yuan *et al.*, *Science* **295**, 102 (2002); published online 13 December 2001; 10.1126/science.1066790.
25. J. Kim, O. Benson, H. Kan, Y. Yamamoto, *Nature* **397**, 500 (1999).
26. S. H. Kim, S. K. Kim, Y. H. Lee, unpublished data.
27. S. Noda, A. Chutinan, M. Imada, *Nature* **407**, 608 (2000).
28. D. G. Deppe, N. Holonyak Jr., *J. Appl. Phys.* **64**, R93 (1988)

29. This work was supported by the National Research Laboratory Project of Korea and the National Research and Development Project for Nano Science and Technology.

Supporting Online Material

www.sciencemag.org/cgi/content/full/305/5689/1444/DC1

Materials and Methods

Figs. S1 to S4

1 June 2004; accepted 29 July 2004

Macroscopic, Neat, Single-Walled Carbon Nanotube Fibers

Lars M. Ericson,[1,2] Hua Fan,[1,2] Haiqing Peng,[1,2] Virginia A. Davis,[1,3] Wei Zhou,[5] Joseph Sulpizio,[1,2] Yuhuang Wang,[1,2] Richard Booker,[1,2] Juraj Vavro,[5] Csaba Guthy,[5] A. Nicholas G. Parra-Vasquez,[1,3] Myung Jong Kim,[1,2] Sivarajan Ramesh,[1,2] Rajesh K. Saini,[1,4] Carter Kittrell,[1,2] Gerry Lavin,[6] Howard Schmidt,[1,2] W. Wade Adams,[1,2] W. E. Billups,[1,4] Matteo Pasquali,[1,3] Wen-Fang Hwang,[1,2]* Robert H. Hauge,[1,2] John E. Fischer,[5] Richard E. Smalley[1,2]*

Well-aligned macroscopic fibers composed solely of single-walled carbon nanotubes (SWNTs) were produced by conventional spinning. Fuming sulfuric acid charges SWNTs and promotes their ordering into an aligned phase of individual mobile SWNTs surrounded by acid anions. This ordered dispersion was extruded via solution spinning into continuous lengths of macroscopic neat SWNT fibers. Such fibers possess interesting structural composition and physical properties.

Individual single-walled carbon nanotubes (SWNTs) possess remarkable mechanical (*1–3*), electrical (*4–6*), and thermal (*7*, *8*) properties that equal, or even surpass, those of other benchmark materials (steel, copper, and diamond, respectively). Applications on the nanometer and micrometer scale, such as SWNT-based transistors (*9*) and chemical sensors (*10*), are progressing rapidly. To date, SWNT composite fibers have been produced that show notable mechanical reinforcement (*11–13*) or improvements in otherwise marginal transport properties (*14*). However, they still fall far short of the impressive properties of individual SWNTs. Neat SWNT fibers have only been produced in relatively short centimeter lengths through laboratory processes with limited industrial scalability (*15–17*), or have been produced in continuous lengths during the nanotube synthesis process, with high levels of impurities and marginal alignment (*18*). Starting with purified SWNTs, we have produced well-aligned continuous macroscopic fibers, without any supporting surfactant or polymer structure. Fibers were made from concentrated dispersions of SWNTs in 102% sulfuric acid via an industrially viable wet spinning technique.

Because of the high temperature stability of SWNTs, melt spinning is not an option. Wet spinning is the only viable approach, as is the case for conventional rodlike polymers such as poly(p-phenylene benzobisoxazole) (PBO), poly(p-phenylene terephthalamide) (PPTA), and poly(p-phenylene benzobisthiazole) (PBZT). The main challenge to the production of neat SWNT fibers is dispersing the SWNTs at high enough concentrations suitable for efficient alignment and effective coagulation. However, because of their chemical inertness and strong intertube van der Waals attractions, SWNTs aggregate into ropes with limited solubility in aqueous, organic, or acidic media. Even in stable organic (such as dimethyl formamide or dichlorobenzene) or surfactant-aided aqueous (such as sodium dodecyl sulfate or Triton X-100) dispersions, SWNTs are typically limited to low concentrations of nanotube bundles. If a surfactant is used to disperse the SWNTs, there is the added complication of removing the surfactant from the fiber during coagulation or after processing. In superacids (100+% sulfuric acid), SWNTs form charge-transfer complexes of individual positively charged nanotubes surrounded by a finite number of sulfuric acid anions (*19*). At very low concentration, such charged tube–anion complexes behave as Brownian rods (*20*). At higher concentration [>0.03 weight % (wt%)], a small amount of dissolved individual tubes coexists with a SWNT spaghetti phase consisting of seemingly endless "swollen" ropes of well-aligned positively charged SWNTs intercalated by sulfuric acid anions (*19*). The SWNTs in the spaghetti are mobile and at a high enough concentration (>4 wt%), they coalesce and form ordered domains (*20*), behaving similarly to nematic liquid crystalline rodlike polymers. The SWNT/acid system is very sensitive to water; the introduction of even minimal moisture causes phase separation and the precipitation of discrete needle-like crystal solvates,

[1]Center for Nanoscale Science and Technology, [2]Carbon Nanotechnology Laboratory, [3]Department of Chemical Engineering, [4]Department of Chemistry, Rice University, Houston, TX 77005, USA. [5]Department of Materials Science and Engineering, University of Pennsylvania, Philadelphia, PA 19104, USA. [6]Carbon Consultations, 15 Wellesley Road, Swarthmore, PA 19081, USA.

*To whom correspondence should be addressed. E-mail: whwang@rice.edu (W.F.H.); smalley@rice.edu (R.E.S.)

termed "SWNT alewives" (*19*, *20*). Using conventional fiber-spinning techniques, this ordered SWNT dispersion can be extruded and coagulated in a controlled fashion to produce continuous lengths of macroscopic neat SWNT fibers (*21*).

SWNTs used in this study were produced by high-pressure decomposition of CO (HiPco) (*22*, *23*) and were purified to remove excess metal catalyst (*24*–*26*). An 8 wt% dispersion of purified SWNTs in 102% sulfuric acid (2 wt% excess SO_3) was prepared in a nitrogen-purged dry box. The mixture was manually mixed and then transferred to the mixing apparatus via a stainless steel syringe. The mixture remained fastidiously dry during transfer and mixing to prevent the formation of SWNT alewives or changes in the acid's protonating ability. Extensive mixing was accomplished by two alternating pneumatic pistons, which pushed the SWNT dope back and forth through an actively rotating shear cell within an evacuated housing (*26*). The speed of the mixing pistons under a constant applied pneumatic pressure allowed for relative changes in dope viscosity to be monitored. When the viscosity reached a steady state, the SWNT material was extruded through a small capillary tube (<125 μm in diameter) into a coagulation bath (Fig. 1B). Fibers were produced under a variety of conditions, including different dope temperatures (0° to 100°C), coagulants (diethyl ether, 5 wt% aqueous sulfuric acid, or water), and coagulation bath temperatures (0°C and room temperature). In the case of aqueous coagulants, fibers were washed for several hours before collection onto a Teflon drum (Fig. 1C). To remove water and residual acid, water-coagulated fibers were dried in a vacuum oven at 100°C, followed by annealing in a flow of H_2/Ar (1:1) at 1 atm and 850°C for 1 hour. Fibers extruded into diethyl ether dried quickly in air. Before conductivity and x-ray diffraction (XRD) measurements, all fibers were further annealed in vacuum at ~1100°C.

Scanning electron micrograph (SEM) images show highly aligned macroscopic fibers consisting solely of SWNTs without any surface contaminants or impurities (Fig. 2, C and D). As in rodlike polymer spinning, the morphology of the fibers was strongly determined by their coagulation conditions. Fibers spun into diethyl ether possessed a collapsed structure (commonly referred to as "dog-bone") due to the rapid flux of sulfuric acid leaving the fiber during the coagulation process. A dense rigid skin formed, which collapsed upon evaporation of the ether, resulting in a fiber of density 0.87 ± 0.08 g/ml. When spun into dilute sulfuric acid or water, the fiber retained its circular shape and coagulated in a more uniform manner (Fig. 2C). These fibers possessed a density of 1.11 ± 0.07 g/ml, which is consistent with more uniform coagulation and fewer internal voids. The fact that the water-coagulated fibers had a density 77% that of the theoretical close-packing density for 1.0-nm nanotubes (1.5 g/ml) is encouraging. In addition to overall morphology, all of the neat fibers possessed an interesting substructure of nanotube super-ropes (Fig. 2D), approximately 200 to 600 nm in diameter. These super-ropes were typically well packed together and possessed connectivity between one another. A closer examination of these super-ropes shows that they are themselves composed of a dense packing of smaller ropes approximately 20 nm in diameter. Similar to the elemental microfibrils commonly observed in many rigid rod polymer fibers, they are believed to be formed during the coagulation of liquid crystalline samples during the extrusion process (*27*).

In addition to the qualitative alignment information that SEM analysis provided, polarized Raman spectroscopy and XRD have been used to probe the degree of alignment (*28*). Because of the anisotropic polarization of SWNTs, the ratio of a SWNT sample's G-band intensity (parallel versus perpendicular) provides a useful probe of the relative degree of alignment and has been used to probe other SWNT objects (*16*, *29*). The neat SWNT fibers possess a Raman ratio greater than 20:1. XRD analysis reveals that both ether-coagulated and water-coagulated fibers are highly aligned, with a full width at half maximum (FWHM) mosaic angle of $\phi = 31°$ and an unaligned fraction less than 10%. In comparison, Fischer *et al.*'s SWNT magnetic assemblies possessed FWHM of $\phi = 33°$, a Raman ratio of 4:1, and an unaligned fraction of 21% (*30*); Wei *et al.*'s vapor-grown SWNT fibers had a $\phi = 75°$ (*31*) and Vigolo *et al.*'s polymer-assisted SWNT fibers possessed FWHM of $\phi = 50°$ (*32*).

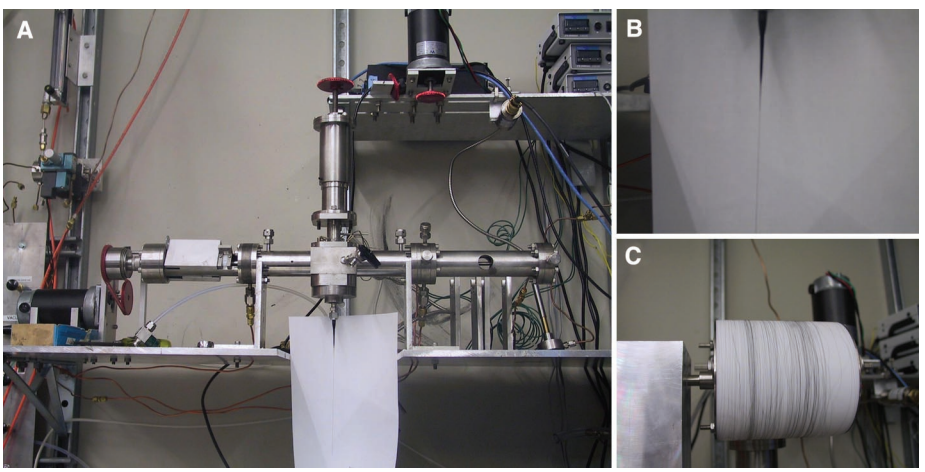

Fig. 1. The spinning process for SWNTs in 102% sulfuric acids. (**A**) The custom-built apparatus used for mixing and extruding neat SWNT fibers. (**B**) A jet of SWNT dispersion being extruded from a capillary tube. (**C**) A 30-m spool of water-coagulated fiber.

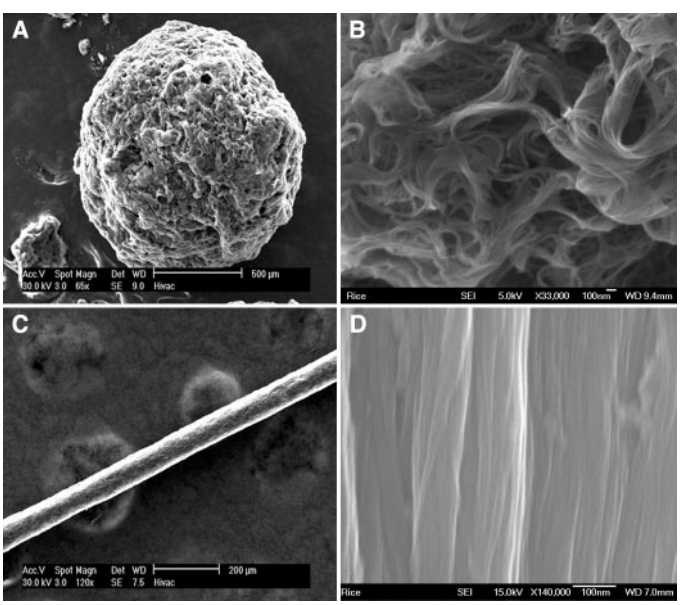

Fig. 2. SEM images showing the evolution of purified SWNTs into continuous fiber. (**A**) SWNTs after the purification process (*24*). (**B**) View inside the purified SWNTs shows a tangled mass of SWNT ropes that are 20 to 30 nm in diameter. (**C**) An annealed neat SWNT fiber spun from 8 wt% dispersion in 102% sulfuric acid and coagulated in water. (**D**) Higher magnification of the neat fiber surface shows that all the ropes have coalesced into aligned super-ropes that are 200 nm or larger in diameter.

The neat SWNT fibers possess good mechanical properties, with a Young's modulus of 120 ± 10 GPa and a tensile strength of 116 ± 10 MPa. The modulus is a good indicator of mechanical performance, because the strength is limited by the presence of localized defects and voids. In comparison, laboratory-grade PBO fibers possess a Young's modulus of 138 GPa and a tensile strength of 2.6 GPa (*11*). The electrical resistivity of the fibers is around ρ = 0.2 milliohm·cm, with an order of magnitude increase upon high-temperature annealing, which removes residual acid and the initial doping (*33*). The thermal conductivity of ether-coagulated fibers is κ = 21 W/K·m. Both conductivities are two orders of magnitude higher than those of SWNT fibers that involve polymers in their production process (*12*), but are similar to those of randomly oriented (*34*) and aligned mats of SWNTs (*30*). Given that the connectivity between SWNTs within a fiber is critical for transport properties and the presence of more than 20% voids, these values are not unexpected.

The success of this fiber-spinning process is predicated on the formation of SWNT/acid charge-transfer complexes (Fig. 3, A and B), which are highly mobile, highly dispersible, and easily align into ordered mesophases in SWNT dopes. This model is further supported by the swelling behavior of SWNT fibers in sulfuric acids. Inside a dry glove box, lengths of neat SWNT fiber were sealed in a quartz cell with sulfuric acid of varying concentrations and observed under an optical microscope. Fibers reexposed at room temperature to 102% or 120% sulfuric acid quickly swelled and sank to the bottom of the cell, whereas fibers exposed to 96% sulfuric acid (that is, concentrated) floated at the top. However, upon heating to 60°C, the fiber in concentrated sulfuric acid swelled and sank to the bottom. The ratio (R) of diameters before and after exposure to sulfuric acid was used to quantify the degree of swelling. In 102% sulfuric acid, ether-coagulated fiber was found to swell to $R = 1.9 \pm 0.1$, whereas the denser, water-coagulated, dried and annealed fibers swelled to $R = 1.66 \pm 0.11$ and 1.33 ± 0.1, respectively (Fig. 3, C and D). In 120% sulfuric acid, $R = 1.96 \pm 0.11$ and 1.44 ± 0.09 for the water-coagulated, dried and annealed fibers, respectively. Because the swelling ratios were less than two, there were probably fewer than three acid layers between adjacent nanotubes.

Given the considerable difference in density between SWNT fibers (< 1.11 g/ml), a close-packed triangular lattice of empty SWNTs (~1.5 g/ml), and sulfuric acid (~1.9 g/ml), the sinking behavior cannot be explained by the idea that sulfuric acid simply fills accessible nanotube voids and swells the fiber. Instead, the sulfuric acid within the fiber must form a dense phase. Sulfuric acid molecules intercalate nanotube ropes within

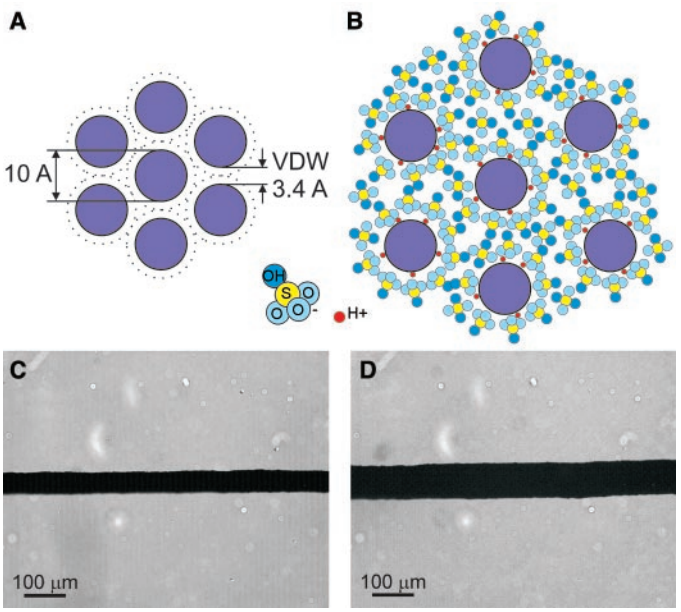

Fig. 3. A model illustrating the swelling of SWNT ropes in sulfuric acid. (**A**) A cartoon of SWNTs in van der Waals (VDW) contact within a neat fiber. (**B**) The same SWNT fiber after reexposure to sulfuric acid. A dense layer of sulfuric acid anions surrounds the individual nanotubes, forming an energetically favorable charge-transfer complex; additional acid molecules fill available voids. The chemical and structural character of the model is meant to be highly schematic. One possible mechanism that generates the repulsive interaction of SWNTs is direct protonation. (**C**) A neat fiber (52.7 μm in diameter) within a quartz cell (**D**) swells to 87.4 μm in diameter ($R = 1.66$) upon exposure to 102% sulfuric acid.

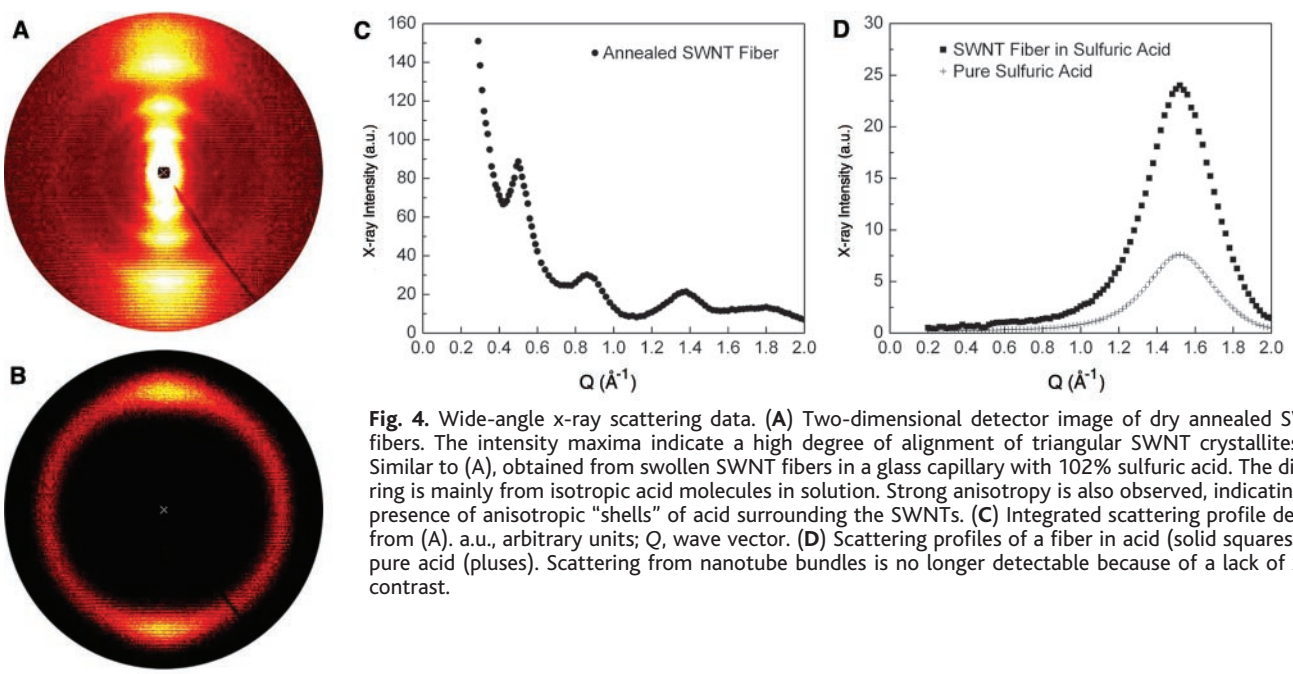

Fig. 4. Wide-angle x-ray scattering data. (**A**) Two-dimensional detector image of dry annealed SWNT fibers. The intensity maxima indicate a high degree of alignment of triangular SWNT crystallites. (**B**) Similar to (A), obtained from swollen SWNT fibers in a glass capillary with 102% sulfuric acid. The diffuse ring is mainly from isotropic acid molecules in solution. Strong anisotropy is also observed, indicating the presence of anisotropic "shells" of acid surrounding the SWNTs. (**C**) Integrated scattering profile derived from (A). a.u., arbitrary units; Q, wave vector. (**D**) Scattering profiles of a fiber in acid (solid squares) and pure acid (pluses). Scattering from nanotube bundles is no longer detectable because of a lack of x-ray contrast.

the fiber and possibly fill the SWNTs, forming charge-transfer complexes with individual nanotubes. The fact that solid sulfuric acid has a density of 2.13 g/ml (*35*) suggests that there is a similar increase in density for the ordered layer of sulfuric acid molecules surrounding the nanotubes (Fig. 3B). XRD data further support this interpretation.

In addition to XRD performed on dry fiber samples, data were also collected on a swollen SWNT fiber sample sealed in a glass capillary with 102% sulfuric acid. The pattern no longer showed the distinct Bragg reflections associated with SWNTs (*4*) in the neat fibers, and the scattering intensity at small angles diminished (Fig. 4), indicating that (i) the intercalation of SWNTs by sulfuric acid smears out the triangular lattice, and (ii) the density, and therefore the electron density, of the acid-swollen fibers has become similar to that of the superacid. Instead, the scattering profile shows only highly anisotropic scattering from the pure 102% sulfuric acid (Fig. 4D) but with about the same degree of orientation (FWHM = 32.1°) as the dry fibers. This means that some of the acid molecules must be aligned with respect to the fiber axis and that the anisotropic scattering is from a cylindrical shell of perhaps three acid monolayers in which the mass density is somewhat enhanced with respect to the bulk liquid because of interactions with the nanotubes. These results further affirm our model of acid-intercalated SWNT ropes in superacids, with individual nanotubes surrounded by ordered layers of sulfuric acid.

References and Notes

1. A. Krishnan, E. Dujardin, T. W. Ebbesen, *Phys. Rev. B* **58**, 14013 (1998).
2. D. A. Walters *et al.*, *Appl. Phys. Lett.* **74**, 3803 (1999).
3. M. F. Yu, B. S. Files, S. Arepalli, R. S. Ruoff, *Phys. Rev. Lett.* **84**, 5552 (2000).
4. A. Thess *et al.*, *Science* **273**, 483 (1996).
5. S. J. Tans *et al.*, *Nature* **386**, 474 (1997).
6. P. L. McEuen, M. S. Fuhrer, H. K. Park, *IEEE Trans. Nanotech.* **1**, 78 (2002).
7. J. Hone, M. Whitney, C. Piskoti, A. Zettl, *Phys. Rev. B* **59**, R2514 (1999).
8. J. Che, T. Cagin, W. A. Goddard, *Nanotechnology* **11**, 65 (2000).
9. R. Seidel *et al.*, *Nano Lett.* **4**, 831 (2004).
10. K. Besteman, J. Lee, F. G. M. Wiertz, H. A. Heering, C. Dekker, *Nano Lett.* **3**, 727 (2003).
11. S. Kumar *et al.*, *Macromolecules* **35**, 9039 (2003).
12. B. Vigolo *et al.*, *Science* **290**, 1331 (2000).
13. A. B. Dalton *et al.*, *Nature* **423**, 703 (2003).
14. R. Andrews *et al.*, *Appl. Phys. Lett.* **75**, 1329 (1999).
15. H. W. Zhu *et al.*, *Science* **296**, 884 (2002).
16. H. H. Gommans *et al.*, *J. Appl. Phys.* **88**, 2509 (2000).
17. K. Jiang, Q. Li, S. Fan, *Nature* **419**, 801 (2002).
18. Y. Li, I. A. Kinloch, A. H. Windle, *Science* **304**, 274 (2004).
19. S. Ramesh *et al.*, *J. Phys. Chem. B* **108**, 8794 (2004).
20. V. A. Davis *et al.*, *Macromolecules* **37**, 154 (2004).
21. R. E. Smalley *et al.*, U.S. Patent Application 20030170166 (2003).
22. P. Nikolaev *et al.*, *Chem. Phys. Lett.* **313**, 91 (1999).
23. M. J. Bronikowski, P. A. Willis, D. T. Colbert, K. A. Smith, R. E. Smalley, *J. Vac. Sci. Technol.* **19**, 1800 (2001).
24. The SWNTs were purified using a protocol based on Chiang *et al.*'s work (*25*). The process involved soft-baking followed by HCl extraction of the metal catalyst. During neutralization of the acid, the nanotube slurry was exchanged multiple times with hexanes in a separation flask. The SWNTs were found to readily move to the hexane layer, leaving aqueous HCl with extracted metal catalyst that was easily drained off. The purified SWNTs possessed less than 1.2 atom % residual metal catalyst, as determined by thermogravimetric analysis. The resulting purified material was a light porous powder with high surface area that could be easily handled (Fig. 1A).
25. I. W. Chiang, B. E. Brinson, R. E. Smalley, J. L. Margrave, R. H. Hauge, *J. Phys. Chem. B* **105**, 1157 (2001).
26. L. M. Ericson, thesis, Rice University, Houston, TX (2003).
27. Y. Tsabba, D. M. Rein, Y. Cohen, *J. Poly. Sci. B* **40**, 1087 (2002).
28. A Renishaw MicroRaman System 1000 with a 780-nm diode laser was used to collect Raman spectra. A multiangle diffractometer equipped with a Cu rotating anode, double-focusing optics, evacuated flight path, and two-dimensional wire detector was used for XRD measurements.
29. G. S. Duesberg, I. Loa, M. Burghard, K. Syassen, S. Roth, *Phys. Rev. Lett.* **85**, 5436 (2000).
30. J. E. Fischer *et al.*, *J. Appl. Phys.* **93**, 2157 (2003).
31. B. Q. Wei *et al.*, *Nano Lett.* **2**, 1105 (2002).
32. B. Vigolo, P. Poulin, M. Lucas, P. Launois, P. Bernier, *Appl. Phys. Lett.* **81**, 1210 (2002).
33. W. Zhou *et al.*, *J. Appl. Phys.* **95**, 649 (2004).
34. J. E. Fischer *et al.*, *Phys. Rev. B* **55**, R4921 (1997).
35. D. R. Allan, S. J. Clark, A. Dawson, P. A. McGregor, S. Parsons, *J. Chem. Soc. Dalton Trans.* **8**, 1867 (2002).

36. This work was supported by the Office of Naval Research (ONR) under the DURINT program, grant N00014-01-1-0789; by ONR N00014-03-1-0890; by U.S. Department of Energy grant DE-FG02-98ER45701; and by the Robert A. Welch Foundation. We thank S. Kumar, K. Winey, and R. Baughman for valuable conversations.

14 June 2004; accepted 30 July 2004

External and Internal Morphology of the BAR 1002′00 *Orrorin tugenensis* Femur

K. Galik,[1] B. Senut,[2] M. Pickford,[3] D. Gommery,[4] J. Treil,[5] A. J. Kuperavage,[6] R. B. Eckhardt[6]*

Late Miocene fossils from the Lukeino Formation in Kenya's Tugen Hills are assigned to *Orrorin tugenensis*. Of 20 fossils recovered there to date, 3 are proximal femurs. One of these, BAR 1002′00, preserves an intact head connected to the proximal shaft by an elongated neck. Although this fossil is comparable in size to *Pan troglodytes*, computerized tomography scans of the neck-shaft junction of BAR 1002′00 reveal that the cortex is markedly thinner superiorly than inferiorly, differing from the approximately equal cortical thicknesses observed in extant African apes, approaching the condition in later hominids, and indicating that *O. tugenensis* was bipedal.

Orrorin tugenensis is thought to represent some of the earliest known hominids, securely dated biostratigraphically, geologically, and radiometrically, as well as by paleomagnetism, to the Late Miocene, approximately 6 million years ago (Ma) (*1*, *2*). Samples (*1*) are derived from four localities in the Lukeino Formation (Aragai, Cheboit, Kapcheberek, and Kapsomin), along the eastern approach to the Tugen Hills in Baringo District, Kenya. Twenty fossils representing at least five individuals have been discovered there. Of these, three are portions of femurs critical for determining posture. BAR 1215′00 is a small fragment consisting of the proximal portion of a right femur lacking neck and head and preserving only about 20 mm of the upper shaft below the base of the greater trochanter, which also is missing. BAR 1003′00 comprises approximately half of a proximal left femur, including the entire lesser trochanter but lacking both the greater trochanter and the femoral head. The third partial femur, BAR 1002′00, is more complete, including about 200 mm of shaft plus an intact head that is connected to the shaft by a somewhat elongated neck; its anatomical features have been described fully and compared in detail with extant African apes and humans, as well as with Plio-Pleistocene hominids (*1*, *3*, *4*).

The Tugen Hills material apparently is younger than the Chad cranium (*Sahelanthropus tchadensis*) from the Toros-Menalla locality (*5*), the age of which is estimated to be in the range of 6 to 7 million years from faunal correlations with East African sites

[1]Orthopedic Biomechanics Laboratory, Allegheny General Hospital, Pittsburgh, PA 15212, USA. [2]Département Histoire de la Terre, Muséum national d'Histoire naturelle, UMR 5143 du CNRS, Case Postale 38, 57, rue Cuvier, 75231 Paris Cedex 05, France. [3]Chaire de Paléoanthropologie et de Préhistoire, Collège de France, et UMR 5143 du CNRS, Département Histoire de la Terre, Muséum national d'Histoire naturelle, UMR 5143 du CNRS, Case Postale 38, 57, rue Cuvier, 75231 Paris Cedex 05, France. [4]UPR 2147 CNRS, 44, rue de l'Amiral-Mouchez, 75014 Paris & GDR 983 du CNRS, 8, rue Buffon, 75005 Paris, France. [5]Service du Radiologie, UMR 8555 du CNRS et Service de Radiologie, Clinique Pasteur, 45, Avenue de Lombez, 31300 Toulouse, France. [6]Laboratory of Comparative Morphology and Mechanics, Department of Kinesiology, Pennsylvania State University, University Park, PA 16802, USA.

*To whom correspondence should be addressed. E-mail: eyl@psu.edu